Available online at www.sciencedirect.com
SCIENCE DIRECT®
Journal of Sound and Vibration 278 (2004) 479–499
JOURNAL OF SOUND AND VIBRATION
www.elsevier.com/locate/jsvi

A flexible multi-body approach for frictional contact in spur gears

O. Lundvall[1], N. Strömberg*, A. Klarbring

Department of Mechanical Engineering, Division of Mechanics, SE-581 83 Linköping, Sweden

Received 20 December 2002; accepted 7 October 2003

Abstract

In the present paper, a large rotational approach for dynamic contact problems with friction is proposed. The approach is used for modelling a spur gear pair with shafts and bearings. The model is obtained by superposing small displacement elasticity on rigid-body motions, and postulating tribological laws on the gear flanks. The finite element method is used to model the elastic properties of the gear pair. Shafts and bearings are represented by linear springs. The tribological laws of the contact interface are Signorini's contact law and Coulomb's law of friction. An important feature of the approach is that the difficulties of impacting mass nodes are avoided. The governing equations of the model are numerically treated by use of the augmented Lagrangian approach. In such manner the geometry of the gear flanks are well represented in the numerical simulations. It is possible to study accurately the consequences of different types of profile modifications as well as flank errors. In this work, the dynamic transmission error is studied. For instance, it turns out that the effect from profile modification is less significant for the transmission error when frictional effects are included.

1. Introduction

A major concern in gear design is gear noise. The main source of gear noise is the appearance of non-uniform rotations of the gear wheels. This is a consequence of deviations from the desired geometry of the flank profiles and the non-rigidity of the gears. The deviations of the flank geometry are a result of the manufacturing process and wear. The non-rigidity gives rise to a periodic mesh stiffness variation since a different number of teeth are in contact during the revolution. The non-uniform rotation will induce vibrations that will be transmitted through

*Corresponding author. Tel.: +46-13-284403; fax: +46-13-281101.
E-mail address: nicst@ikp.liu.se (N. Strömberg).
[1] Also at Scania CV AB, SE-151 87 Södertälje, Sweden.

0022-460X/$ - see front matter © 2003 Elsevier Ltd. All rights reserved.
doi:10.1016/j.jsv.2003.10.057

shafts and bearings to the gearbox housing. Another source of excitation is friction. In this work, a flexible multi-body approach for dynamic contact problem with friction is suggested. The approach is utilised in order to study how flank geometry, non-rigidity and friction influence the level of noise in a gear problem. In particular, the dynamic transmission error for a spur gear pair with shafts and bearings is studied.

In order to compare different gear designs with respect to gear noise, the transmission error is used. The transmission error is defined as the difference between the actual position of the gear and its position according to the gear ratio. Consequently, a time-varying transmission error implies a non-uniform rotation of the gear even though the pinion rotates at a constant speed. It is well-known that a larger peak-to-peak value of the transmission error usually results in a higher noise level, see e.g. Ref. [1]. The transmission error is called the static transmission error for quasi-static mesh cycles. When dynamic effects are included the measure is called the dynamic transmission error.

To predict the dynamic response of a gear system, a common procedure in gear design is to calculate the static transmission error followed by a harmonic response analysis. Models of this kind, which in the most simple case consist of two masses and a spring, representing the mean mesh stiffness, are discussed in Ref. [2]. In Ref. [3] a non-linear dynamic gear model, consisting of the two gear wheel bodies, is analysed. The infinitesimal displacement field governed by the finite element method was superposed on prescribed rigid-body motions. A more general approach is used in Ref. [4] where the rigid-body motions were regarded as unknowns. The method was applied to planetary gear trains. Another approach is used in Ref. [5] where a lumped parameter model represents the complete gear system. The contact interface is represented by a set of independent springs along the contact line and corresponding initial gaps. In Refs. [6–8] the effect of friction on the dynamics for a gear pair was studied by lumped parameter models. Examples of more recent works, where friction excitations in gears have been studied, are Refs. [9,10].

The objective in this work is to investigate the dynamic response of a spur gear pair with shafts and bearings when the effect from friction is also included. For that purpose a large rotational approach including Signorini contact and Coulomb friction is suggested. The total motion is defined by superposing small displacement elasticity on rigid-body motions. The inertia of each gear is represented by a point mass and a mass moment of inertia at its centre. The elastic properties of the gears are obtained by using the finite element method. The contact and friction laws of the contact interfaces between the gear flanks are formulated directly in the nodal degrees of freedom of the finite element model. Time integration is carried out by applying the average acceleration method such that no numerical dissipation is generated. The fact that there is no mass associated with the nodal points of the finite element model is an important feature as the average acceleration method is used. In Ref. [11] it is clearly demonstrated that by applying the average acceleration method in connection with a contact formulation of the type used here might cause energy growth in the system. However, this phenomenon is restricted to the case when mass is associated with the impacting nodes which, of course, is not the case in the formulation presented here as inertia is treated in a rigid-body fashion.

In the presented model, the motion of the input shaft is kept homogenous and the exciting source then originates from the geometry of the gear flanks and the mesh-stiffness variation, which are the main components of the static transmission error. Furthermore, as friction is included, the sliding condition between the gear flanks is also a source of excitation. Obviously,

one requirement for obtaining the correct excitation is to represent the geometry of the mating gear flanks accurately. Another requirement is that the sliding conditions between the gear flanks are predicted accurately. In Refs. [12,13] an augmented Lagrangian method was developed where these requirements can be met. The method was further developed and implemented in Ref. [14] for solving fretting problems. In Ref. [15] it was numerically shown that this method is superior to an interior point method both in performance and robustness. Later, the method was successfully applied to gear problems [16,17]. In the latter work, the method was used to calculate the static transmission error. In the present paper the augmented Lagrangian approach is utilised to solve the governing equations of the dynamic gear problem discussed above. In particular, the dynamic transmission error and friction force excitation are studied.

2. The dynamic gear problem

A flexible multi-body approach for dynamic contact problems with friction is suggested.[2] The approach is used for modelling a gear pair with shafts and bearings, see Fig. 1. The model is obtained by superposing small displacement elasticity on rigid-body motions. The pinion mounted on the right shaft is denoted gear $i = 1$ and the wheel mounted on the left shaft is denoted gear $i = 2$. The spatial position of a material point of gear i, represented by a position vector $\mathbf{X}^i$ relative to the centre of the gear, is given by

$$\mathbf{x}^i = \mathbf{Q}^i\mathbf{X}^i + \mathbf{c}^i + \mathbf{u}^i, \tag{1}$$

where

$$\mathbf{Q}^i = \mathbf{Q}^i(\theta^i(t)) = \begin{bmatrix} \cos\theta^i & -\sin\theta^i & 0 \\ \sin\theta^i & \cos\theta^i & 0 \\ 0 & 0 & 1 \end{bmatrix} \tag{2}$$

is a rotation matrix. Here, θ^1 is an angle, which is a given function of time t, that represents the rotation of the right end of the right shaft, see Fig. 1. Consequently, the input torque is taken as an unknown quantity. This is in accordance with the assumption made in Ref. [7], where it is pointed out that gears cannot be assumed to operate under constant input and output torque when friction is included. If no elastic deformations are present and the gear flanks are perfect involutes, then the left shaft has a rotation θ^2 which is defined by

$$\theta^2 Z^2 = -\theta^1 Z^1, \tag{3}$$

where Z^i is the number of teeth on gear i. The vector $\mathbf{c}^i$ defines the centre of the gear and the vector $\mathbf{u}^i = \mathbf{u}^i(\mathbf{Q}^i\mathbf{X}^i, t)$ is the displacement due to elastic deformations, see Fig. 1. In this paper, the applied rotation is assumed to be a linear function of time, i.e., $\theta^1 = \omega^1 t$ where ω^1 is a constant angular velocity.

The elastic deformations of the centre of gear i are represented by $\mathbf{d}_q^i = \{d_x^i, d_y^i, \varphi^i\}^{\mathrm{T}}$, such that the total rotation is $\varphi^i + \theta^i$ and $\mathbf{u}^i(\mathbf{0}, t) = d_x^i\mathbf{e}_x + d_y^i\mathbf{e}_y$. Here, the infinitesimal rotations φ^i are not

[2] A presentation of flexible multi-body approaches can be found in e.g. Ref. [18], and presentations of computational contact mechanics can be found in e.g. Refs. [19,20].

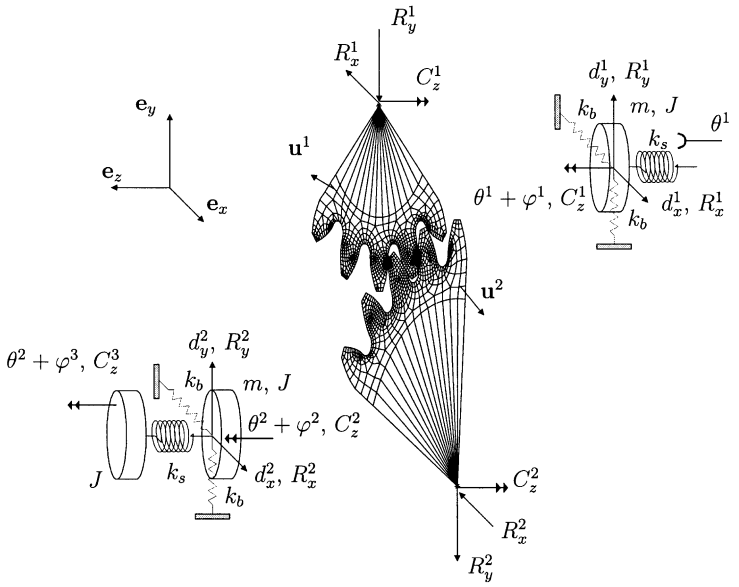

Fig. 1. A gear pair with shafts and bearings.

only due to elastic deformations, but also due to deviations in flank geometry from perfect involutes. Furthermore, T denotes the transpose of a vector or a matrix and $\mathbf{e}_x$, $\mathbf{e}_y$ and $\mathbf{e}_z$ are unit vectors in the x, y and z directions, see Fig. 1. The unit vectors are oriented in such manner that the line of action is orthogonal to $\mathbf{e}_z$. In the numerical simulations, it is assumed that $\mathbf{e}_x$ coincides with the line of action. Except for the prescribed rotation θ^1, the degrees of freedom at the right end point of the right shaft are fixed. The left point of the left shaft is fixed in translation and its total rotational position is $\theta^2+\varphi^3$.

The inertia of each gear is in the model manifested through a lumped mass at each centre and a mass moment of inertia about the $\mathbf{e}_z$-axis. For simplicity, both gears are assumed to have the same mass and the same mass moment of inertia, denoted by m and J, respectively. The mass of the left shaft is manifested by a mass moment of inertia J about the $\mathbf{e}_z$-axis located at the left end point of the left shaft.

A torsional spring, with a spring constant k_s, and two translational springs, both with a spring constant k_b, are attached to the centre of each wheel, representing the stiffness of the shafts and the bearings. The arrangement of the translational springs indicates that any cross coupling term of the bearings are assumed to be zero. According to Ref. [6], this is a most reasonable approximation. A constant force couple C_z^3 is applied to the left end of the lower torsional spring.

The laws of motion for the right shaft read (here it has been taken into account that $\ddot{\theta}^1=0$)

$$\begin{aligned}
&\mathbf{e}_x\text{: } R_x^1 - k_b d_x^1 = m\ddot{d}_x^1,\\
&\mathbf{e}_y\text{: } R_y^1 - k_b d_y^1 = m\ddot{d}_y^1,\\
&\mathbf{e}_z\text{: } C_z^1 - k_s\varphi^1 = J\ddot{\varphi}^1,
\end{aligned} \tag{4}$$

where $\mathbf{R}_q^1 = \{R_x^1, R_y^1, C_z^1\}^{\mathrm{T}}$ are reactions from the centre of the upper gear. Here and in sequel we let a superimposed dot represents the time derivative and a double dot stands for the second time derivative.

The laws of motion for the left shaft can be expressed as (taking into account that $\ddot{\theta}^2 = 0$)

$$\begin{aligned} &\mathbf{e}_x\colon R_x^2 - k_b d_x^2 = m\ddot{d}_x^2,\\ &\mathbf{e}_y\colon R_y^2 - k_b d_y^2 = m\ddot{d}_y^2,\\ &\mathbf{e}_z\colon C_z^2 - k_s(\varphi^2 - \varphi^3) = J\ddot{\varphi}^2 \end{aligned} \tag{5}$$

and

$$\mathbf{e}_z\colon C_z^3 - k_s(\varphi^3 - \varphi^2) = J\ddot{\varphi}^3. \tag{6}$$

Here, $\mathbf{R}_q^2 = \{R_x^2, R_y^2, C_z^2\}^{\mathrm{T}}$ are reactions from the centre of the lower gear.

Even though the mass of the gears is represented in a rigid-body fashion, the elastic properties are modelled in more detail. These are obtained by performing finite element discretisations of the rigid-body configurations of the gears. On these configurations, defined by $\mathbf{Q}^i\mathbf{X}^i + \mathbf{c}^i$, a small displacement formulation is added using isotropic elasticity. Plain strain is assumed. The contact between the gears is treated using a common potential contact surface, obtained by a node-to-node discretisation, which is a standard technique in small displacement contact mechanics, see e.g. Ref. [21]. A typical finite element mesh of the gears used in the numerical calculations is reproduced in Fig. 1. It is important to understand that a benefit of this flexible multi-body approach is the avoidance of impacting mass nodes. The difficulties of impacting mass nodes are discussed in Ref. [19]. For a more detailed presentation of the finite element treatment outlined below, see e.g. Ref. [21].

The resulting stiffness equation of each gear can be written as

$$\begin{bmatrix} \mathbf{K}_{cc}^i & \mathbf{K}_{cd}^i & \mathbf{K}_{cq}^i \\ \mathbf{K}_{dc}^i & \mathbf{K}_{dd}^i & \mathbf{K}_{dq}^i \\ \mathbf{K}_{qc}^i & \mathbf{K}_{qd}^i & \mathbf{K}_{qq}^i \end{bmatrix} \begin{Bmatrix} \mathbf{u}_c^i \\ \mathbf{u}_d^i \\ \mathbf{d}_q^i \end{Bmatrix} + \begin{Bmatrix} \mathbf{F}_c^i \\ \mathbf{0} \\ \mathbf{0} \end{Bmatrix} = \begin{Bmatrix} \mathbf{0} \\ \mathbf{0} \\ -\mathbf{R}_q^i \end{Bmatrix}, \tag{7}$$

where $\mathbf{K}_{cc}^i = \mathbf{K}_{cc}^i(t)$, $\mathbf{K}_{cd}^i = \mathbf{K}_{cd}^i(t)$, etc. are stiffness matrices. Note that $\mathbf{u}_c^i$ and $\mathbf{u}_d^i$ are column vectors, related to and formed from, but not to be confused with, the geometric three-dimensional vector $\mathbf{u}^i$. A subscript c corresponds to nodal degrees of freedom at the potential contact surface, q corresponds to the freedoms at the centre of the gear and d corresponds to all the other finite element displacement freedoms. Note also that stiffness matrices are strictly related to a certain rigid-body configuration and may, thus, be seen as functions of $\theta^i(t)$. Furthermore, the following principle of action and reaction is used:

$$\mathbf{F}_c^1 = -\mathbf{F}_c^2 = \mathbf{C}_n^{\mathrm{T}}\mathbf{P}_n + \mathbf{C}_t^{\mathrm{T}}\mathbf{P}_t, \tag{8}$$

where $\mathbf{P}_n = \{p_{jn}\}$ is the normal contact force vector and $\mathbf{P}_t = \{p_{jt}\}$ is the tangential contact force vector. Matrices $\mathbf{C}_n$ and $\mathbf{C}_t$ are transformation matrices defined by the normal and the tangential direction of the contact surface. The geometry of the spur involute gears implies that these

matrices are constant in time as well as in space, see Refs. [16,17]. By utilising $\mathbf{C}_n$ and $\mathbf{C}_t$, the normal displacement u_{jn}^i and the tangential displacement u_{jt}^i of a contact node j can be obtained by

$$u_{jn}^i = \mathbf{C}_{jn}\mathbf{u}_c^i \quad \text{and} \quad u_{jt}^i = \mathbf{C}_{jt}\mathbf{u}_c^i,$$

where $\mathbf{C}_{jn}$ and $\mathbf{C}_{jt}$ are the jth rows of $\mathbf{C}_n$ and $\mathbf{C}_t$, respectively.

The unilateral contact law can now be formulated as

$$p_{jn} \geqslant 0, \quad \mathbf{C}_{jn}\bar{\mathbf{u}}_c - g_j \leqslant 0, \quad p_{jn}(\mathbf{C}_{jn}\bar{\mathbf{u}}_c - g_j) = 0, \tag{9}$$

by using the relative contact displacement $\bar{\mathbf{u}}_c = \mathbf{u}_c^1 - \mathbf{u}_c^2$ and the initial contact gap

$$g_j = \mathbf{C}_{jn}\{\{\mathbf{Q}^2\mathbf{X}^2 + \mathbf{c}^2\}_c - \{\mathbf{Q}^1\mathbf{X}^1 + \mathbf{c}^1\}_c\},$$

where $\{\mathbf{Q}^i\mathbf{X}^i + \mathbf{c}^i\}_c$ represents the column vectors of the rigid-body positions of the contact nodes.

Furthermore, by introducing the relative tangential velocity

$$\dot{w}_{jt} = \mathbf{C}_{jt}(\dot{\mathbf{x}}_c^1 - \dot{\mathbf{x}}_c^2), \tag{10}$$

the law of friction is expressed by[3]

$$|\dot{w}_{jt}|p_{jt} = \dot{w}_{jt}\mu(p_{jn})_+, \quad |p_{jt}| \leqslant \mu(p_{jn})_+, \tag{11}$$

where μ is the coefficient of friction and $2(x)_+ = x + |x|$ is used. In Eq. (10), $\dot{\mathbf{x}}_c^i$ are column vectors formed from the time derivative of (1), i.e.,

$$\dot{\mathbf{x}}^i = \omega^i\mathbf{e}_z \times \mathbf{Q}^i\mathbf{X}^i + \dot{\mathbf{u}}^i, \tag{12}$$

where $\times$ stands for the vector product. Note that $\dot{\mathbf{u}}^i$ is the material time derivative where $\mathbf{X}^i$ is kept fixed.

The dynamic gear problem has now been stated in Eqs. (4)–(7), (9) and (11). That is, on a time interval $[0, T] \ni t$, find $t \mapsto \mathbf{u}_c^i$, $t \mapsto \mathbf{u}_d^i$, $t \mapsto \mathbf{d}_q^i$, $t \mapsto \mathbf{F}_c^i$ and $t \mapsto \mathbf{R}_q^i$ such that these equations are satisfied for the prescribed rotation $\theta^1 = \omega_1 t$ and the constant force couple C_z^3. In particular, the authors are interested in investigating the following quantity:

$$T_E = (\theta^2 + \varphi^2) + \frac{Z^1}{Z^2}(\theta^1 + \varphi^1) = \varphi^2 + \frac{Z^1}{Z^2}\varphi^1, \tag{13}$$

defining the transmission error. The numerical treatment of the problem is outlined in the following sections.

3. Time discretisation

The dynamic gear problem is solved by introducing discretisations in time. The authors want to formulate an incremental problem which utilises known quantities at time t_n to calculate quantities at time t_{n+1}. Note that the rigid-body configuration at time t_{n+1} is trivial to calculate and the difficulty lies in calculating the elastic deformations at this time. Accelerations appearing

[3] This is a useful formulation of Coulomb's friction law. That is, if $\dot{w}_{jt} = 0$, then $|p_{jt}| \leqslant \mu p_{jn}$, but if $\dot{w}_{jt} \neq 0$, then $p_{jt} = \mu p_{jn}\mathrm{sgn}(\dot{w}_{jt})$.

in Eqs. (4)–(6) are approximated using the average acceleration method:

$$\mathbf{d}_q^i(t_{n+1}) = \mathbf{d}_q^i(t_n) + \frac{\Delta t}{2}\{\dot{\mathbf{d}}_q^i(t_n) + \dot{\mathbf{d}}_q^i(t_{n+1})\},$$
$$\dot{\mathbf{d}}_q^i(t_{n+1}) = \dot{\mathbf{d}}_q^i(t_n) + \frac{\Delta t}{2}\{\ddot{\mathbf{d}}_q^i(t_n) + \ddot{\mathbf{d}}_q^i(t_{n+1})\}, \tag{14}$$

where $\Delta t = t_{n+1} - t_n$ is the time step. Velocities appearing in Eq. (10) is treated by using a backward Euler approximation for $\dot{\mathbf{u}}^i$, i.e.,

$$\dot{\mathbf{u}}^i \simeq \frac{\mathbf{u}^i(\mathbf{Q}^i(t_{n+1})\mathbf{X}^i, t_{n+1}) - \mathbf{u}^i(\mathbf{Q}^i(t_n)\mathbf{X}^i, t_n)}{\Delta t}. \tag{15}$$

The rotation matrices $\mathbf{Q}^i(t_{n+1})$ define the rigid-body configuration at time t_{n+1}. They are directly obtained from the definition in Eq. (2) and the angular velocities ω^1 and ω^2, where the latter is, of course, defined by $\omega^2 Z^2 = -\omega^1 Z^1$, see Eq. (3). To obtain the last term in Eq. (15) is not as trivial as it may seem. In fact, a difficulty arises here due to the finite element discretisation. Since a node-to-node contact treatment requires remeshing, a new mesh and a new potential contact surface are defined on the corresponding rigid-body configuration for every new time t_{n+1}. Consequently, if a contact node is located at $\mathbf{X}^i$ at time t_{n+1}, a node is not necessarily, and probably not, located at this material point in the finite element mesh corresponding to time t_n. This difficulty is treated by introducing an interpolation, see Appendix A.

Inserting Eq. (14) in Eq. (4) yields

$$\mathbf{K}^1 \mathbf{d}_q^1(t_{n+1}) = \mathbf{R}_q^1 + \mathbf{F}^1, \tag{16}$$

where

$$\mathbf{K}^1 = \begin{bmatrix} \frac{4m}{\Delta t^2} + k_b & 0 & 0 \\ 0 & \frac{4m}{\Delta t^2} + k_b & 0 \\ 0 & 0 & \frac{4J}{\Delta t^2} + k_s \end{bmatrix} \tag{17}$$

and

$$\mathbf{F}^1 = \begin{Bmatrix} m\left(\frac{4d_x^1(t_n)}{\Delta t^2} + \frac{4\dot{d}_x^1(t_n)}{\Delta t} + \ddot{d}_x^1(t_n)\right) \\ m\left(\frac{4d_y^1(t_n)}{\Delta t^2} + \frac{4\dot{d}_y^1(t_n)}{\Delta t} + \ddot{d}_y^1(t_n)\right) \\ J\left(\frac{4\varphi^1(t_n)}{\Delta t^2} + \frac{4\dot{\varphi}^1(t_n)}{\Delta t} + \ddot{\varphi}^1(t_n)\right) \end{Bmatrix}. \tag{18}$$

Furthermore, by inserting Eq. (14) in Eqs. (5) and (6) and eliminating $\varphi^3(t_{n+1})$, one obtains

$$\mathbf{K}^2 \mathbf{d}_q^2(t_{n+1}) = \mathbf{R}_q^2 + \mathbf{F}^2, \tag{19}$$

where

$$\mathbf{K}^2 = \begin{bmatrix} \dfrac{4m}{\Delta t^2} + k_b & 0 & 0 \\ 0 & \dfrac{4m}{\Delta t^2} + k_b & 0 \\ 0 & 0 & \dfrac{4J}{\Delta t^2} + \dfrac{4Jk_s}{4J + \Delta t^2 k_s} \end{bmatrix} \tag{20}$$

and

$$\mathbf{F}^2 = \begin{Bmatrix} m\left(\dfrac{4d_x^2(t_n)}{\Delta t^2} + \dfrac{4\dot{d}_x^2(t_n)}{\Delta t} + \ddot{d}_x^2(t_n)\right) \\ m\left(\dfrac{4d_y^2(t_n)}{\Delta t^2} + \dfrac{4\dot{d}_y^2(t_n)}{\Delta t} + \ddot{d}_y^2(t_n)\right) \\ J\left(\dfrac{4\varphi^2(t_n)}{\Delta t^2} + \dfrac{4\dot{\varphi}^2(t_n)}{\Delta t} + \ddot{\varphi}^2(t_n)\right) + \cdots \\ \dfrac{Jk_s\Delta t^2}{4J + \Delta t^2 k_s}\left(\dfrac{4\varphi^3(t_n)}{\Delta t^2} + \dfrac{4\dot{\varphi}^3(t_n)}{\Delta t} + \ddot{\varphi}^3(t_n)\right) + \dfrac{\Delta t^2 k_s C_z^3}{4J + \Delta t^2 k_s} \end{Bmatrix}. \tag{21}$$

Eqs. (7), (16) and (19) are put together in order to eliminate $\mathbf{d}_q^i(t_{n+1})$ and $\mathbf{R}_q^i$. The result is

$$\begin{bmatrix} \mathbf{K}_{cc}^i - \mathbf{K}_{cq}^i\mathbf{K}_{inv}^i\mathbf{K}_{qc}^i & \mathbf{K}_{cd}^i - \mathbf{K}_{cq}^i\mathbf{K}_{inv}^i\mathbf{K}_{qd}^i \\ \mathbf{K}_{dc}^i - \mathbf{K}_{dq}^i\mathbf{K}_{inv}^i\mathbf{K}_{qc}^i & \mathbf{K}_{dd}^i - \mathbf{K}_{dq}^i\mathbf{K}_{inv}^i\mathbf{K}_{qd}^i \end{bmatrix} \begin{Bmatrix} \mathbf{u}_c^i \\ \mathbf{u}_d^i \end{Bmatrix} + \begin{Bmatrix} \mathbf{F}_c^i \\ \mathbf{0} \end{Bmatrix} + \begin{Bmatrix} \mathbf{K}_{cq}^i\mathbf{K}_{inv}^i\mathbf{F}^i \\ \mathbf{K}_{dq}^i\mathbf{K}_{inv}^i\mathbf{F}^i \end{Bmatrix} = \begin{Bmatrix} \mathbf{0} \\ \mathbf{0} \end{Bmatrix}, \tag{22}$$

where $\mathbf{K}_{inv}^i = [\mathbf{K}_{qq}^i + \mathbf{K}^i]^{-1}$. Note here that Eq. (7) is evaluated at time t_{n+1}, i.e., at $\theta^i(t_{n+1})$.

Finally, putting Eqs. (12) and (15) in Eq. (10) results in

$$\dot{w}_{jt} \simeq \mathbf{C}_{jt}\mathbf{v}_c^{rigid} + \mathbf{C}_{jt}\left\{\frac{\mathbf{u}_c^1(t_{n+1}) - \mathbf{u}_c^2(t_{n+1})}{\Delta t} - \frac{\mathbf{u}_c^1(t_n) - \mathbf{u}_c^2(t_n)}{\Delta t}\right\}, \tag{23}$$

where $\mathbf{v}_c^{rigid}$ is the part of the relative velocity that is due to the rigid-body motion. It is calculated by forming a column vector from the geometric vector $\omega^1\mathbf{e}_z \times \mathbf{Q}^1\mathbf{X}^1 - \omega^2\mathbf{e}_z \times \mathbf{Q}^2\mathbf{X}^2$.

4. Augmented Lagrangian formulation

The equations to be solved are now given by Eqs. (9), (11) and (22), where in addition expressions in Eqs. (8), (12) and (23) are also needed. The solution is obtained by reformulating these equations as an augmented Lagrangian system of equations which in turn is solved using a non-smooth Newton method. This approach has proven to be very successful for solving friction problems, see e.g. Refs. [14–17,22–24]. Most recently, the approach was utilised to solve dynamic wear problems in Ref. [25]. The approach is briefly discussed below. Details can be found in the references just cited.

The main idea of the approach is to reformulate the contact and friction laws defined by Eqs. (9) and (11) as equivalent non-smooth equations. These equations are

$$p_{jn} = (p_{jn} + r(\mathbf{C}_{jn}\bar{\mathbf{u}}_c - g_j))_+, \tag{24}$$

$$p_{jt} = \begin{cases} p_{jt} + r(\mathbf{C}_{jt}\bar{\mathbf{u}}_c + w_{jt}^{old}) & \text{if } |p_{jt} + r(\mathbf{C}_{jt}\bar{\mathbf{u}}_c + w_{jt}^{old})| \leqslant \mu(p_{jn})_+, \\ \mu(p_{jn})_+ \operatorname{sgn}(p_{it} + r(\mathbf{C}_{jt}\bar{\mathbf{u}}_c + w_{jt}^{old})) & \text{otherwise,} \end{cases} \tag{25}$$

where

$$w_{jt}^{old} = \Delta t \mathbf{C}_{jt}\mathbf{v}_c^{rigid} - \mathbf{C}_{jt}\bar{\mathbf{u}}_c(t_n).$$

These equations are, of course, treated fully implicitly, i.e., $\bar{\mathbf{u}}_c = \bar{\mathbf{u}}_c(t_{n+1})$.

The dynamic gear problem is now presented as an augmented Lagrangian formulation by Eqs. (22) and (24)–(25). This system of equations is solved by using the Newton algorithm presented in Appendix B. When the method is implemented the equilibrium equation (22) is reduced even further by performing a static condensation such that it is expressed using $\bar{\mathbf{u}}_c$ as the only unknown instead of using $\mathbf{u}_c^i$ and $\mathbf{u}_d^i$, see Appendix C.

5. Numerical results

The numerical method outlined above is used to calculate the transmission error defined in Eq. (13). The transmission error is studied for different mesh frequencies ($f_m = \omega^1 Z^1/2\pi$) and different amount of profile modification (see Fig. 7). Results are presented both for cases with friction ($\mu = 0.1$) and without friction ($\mu = 0$). In the calculations, extra system damping is added in order to represent viscosity of oil and friction in bearings. For each shaft regarded alone Rayleigh damping is assumed. By applying Rayleigh damping, Eqs. (4), (5) and(6) are modified to read

$$\begin{aligned} &\mathbf{e}_x\colon R_x^1 - k_b d_x^1 - (\alpha k_b + \beta m)\dot{d}_x^1 = m\ddot{d}_x^1, \\ &\mathbf{e}_y\colon R_y^1 - k_b d_y^1 - (\alpha k_b + \beta m)\dot{d}_y^1 = m\ddot{d}_y^1, \\ &\mathbf{e}_z\colon C_z^1 - k_s\varphi^1 - (\alpha k_s + \beta J)\dot{\varphi}^1 = J\ddot{\varphi}^1, \end{aligned} \tag{26}$$

$$\begin{aligned} &\mathbf{e}_x\colon R_x^2 - k_b d_x^2 - (\alpha k_b + \beta m)\dot{d}_x^2 = m\ddot{d}_x^2, \\ &\mathbf{e}_y\colon R_y^2 - k_b d_y^2 - (\alpha k_b + \beta m)\dot{d}_y^2 = m\ddot{d}_y^2, \\ &\mathbf{e}_z\colon C_z^2 - k_s(\varphi^2 - \varphi^3) - \beta J\dot{\varphi}^2 - \alpha k_s(\dot{\varphi}^2 - \dot{\varphi}^3) = J\ddot{\varphi}^2 \end{aligned} \tag{27}$$

and

$$\mathbf{e}_z\colon \quad C_z^3 - k_s(\varphi^3 - \varphi^2) - \beta J\dot{\varphi}^3 - \alpha k_s(\dot{\varphi}^3 - \dot{\varphi}^2) = J\ddot{\varphi}^3. \tag{28}$$

This modification does not significantly affect the numerical treatment outlined in the previous section.

If Rayleigh damping is excluded, global loss of contact is obtained. This implies that large values of T_E are calculated, indicating that the unloaded flanks at the opposite side of the gear

Table 1
Model data

α	0.4×10^{-3}	s
β	0.5×10^{-3}	1/s
J	24.5	kgmm^2
m	4.9×10^{-3}	Ns^2/mm
k_b	0.155×10^6	N/mm
k_s	0.203×10^9	Nmm/rad
C_z^3	0.437×10^6	Nmm
E	2.06×10^5	N/mm^2
v	0.3	

Table 2
Gear data (see e.g. Ref. [1])

Centre distance	91.5 mm	
Module	4.5 mm	
Pressure angle	20°	
	Pinion	Gear
Number of teeth	16	24
Pitch diameter	73.2 mm	109.8 mm
Outside diameter	82.64 mm	118.64 mm
Root diameter	62.50 mm	98.37 mm
Tooth width	15.0 mm	15.0 mm
Addendum mod. coef.	0.196	0.125

teeth would come into contact. Since these flanks are not considered to be parts of the potential contact surface such results can not be regarded as physical solutions.

Model data are listed in Tables 1 and 2, where gear data is contained in the latter. Gear data are identical to those used in Ref. [17]. The commercial finite element program Ansys 5.7 is used to generate the stiffness matrices. A four noded plane strain element (Plane42) is used with extra displacement shapes included. Young's modulus, E, and Poisson ratio, v, are given in Table 1. In the numerical implementation the base vectors $\mathbf{e}_x$ and $\mathbf{e}_y$ are assumed to coincide with the normal and tangential direction of the contact interface. That is, $\mathbf{e}_x$ coincides with the line of action, and $\mathbf{e}_y$ is parallel to the off-line of action. Furthermore, depending on the number of teeth in contact, 20–40 contact nodes are used. The length of each contact interface is 1.5 mm.

First, the influence of friction on the transmission error is studied for the quasi-static case. The quasi-static solution is approximated by choosing a sufficiently small value of the mesh frequency ($f_m = 0.01$ Hz). In Fig. 2, where two quasi-static cases are compared, the influence on T_E and d_y^2 from friction is viewed. In the case without friction there is no global tangential displacement at all. To explain the curves in Fig. 2 look at Fig. 3 where an ideal picture is given of the total friction force P_t for two different time instants. In this figure r_{bp} denotes the so-called base pitch. In Fig. 3(a), two flank pairs are in contact. The resulting moment is then $r_{bp}P_t/2$ and the resulting friction force is zero. The latter explains why d_y^2 is approximately zero at the beginning of a mesh

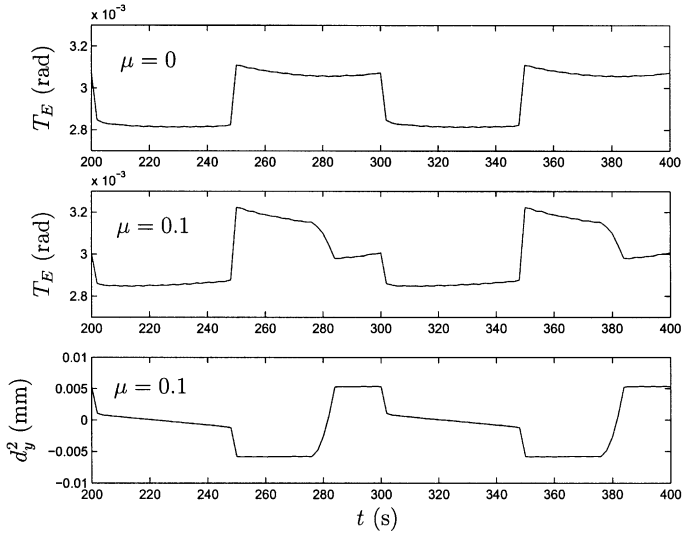

Fig. 2. Static transmission error and shaft deflection d_y^2 of the left shaft (two mesh cycles).

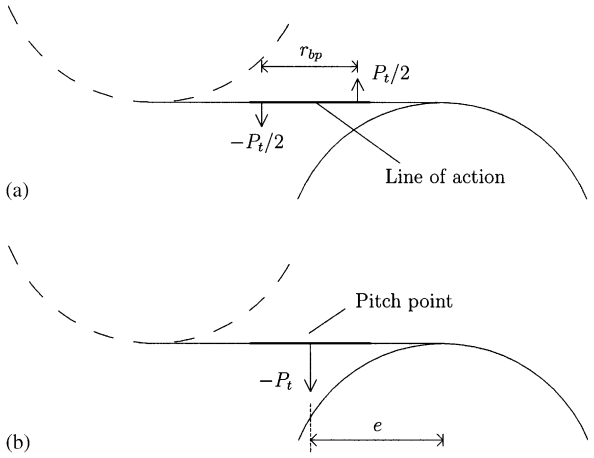

Fig. 3. Friction forces on the gear (to the right). In (a) two flank pairs are in contact and in (b) only one flank pair is in contact.

cycle. In Fig. 3(b), only one flank pair is in contact. As the point of contact moves across the pitch point the resulting moment goes from eP_t to $-eP_t$ and the resulting force form $-P_t$ to P_t. Looking at d_y^2 at the end of a mesh cycle in Fig. 2, this is clearly seen. For the specific gear data, approximate values of r_{bp} and $\mathbf{e}$ are 13.3 and 21.0 mm, respectively. Clearly, torque is transmitted via friction. As C_z^3 is constant, the line of action force and the off line of action force interact in order to balance this torque in the quasi-static case. Accordingly, this interaction will not only influence the reaction forces R_x^1 and R_y^1 but also C_z^1, see Fig. 4. When friction is included, a sudden change in the static transmission error is seen at the end of a mesh cycle, cf. Fig. 2. This is due to the fact that it is possible for the centre of a gear wheel to be displaced. Because of the

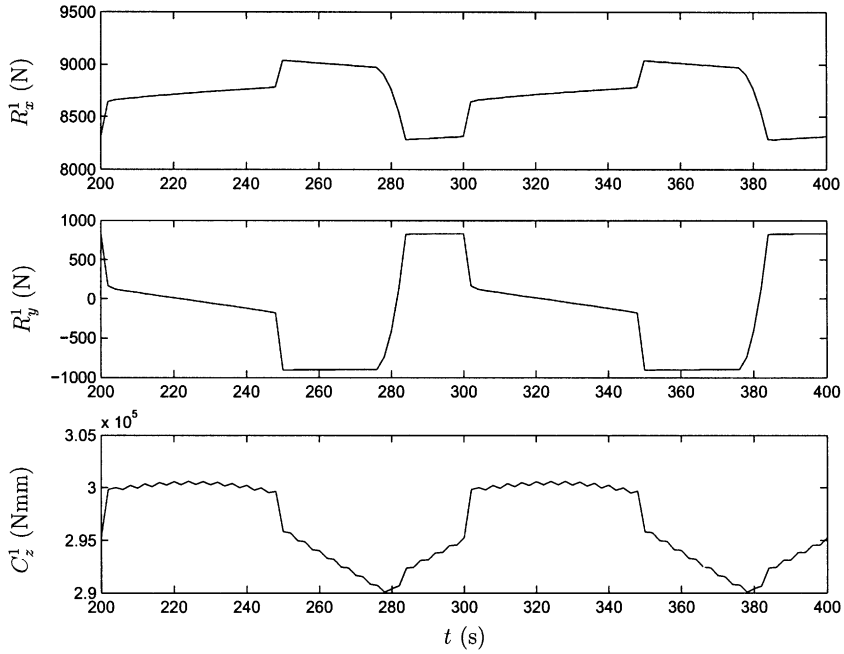

Fig. 4. Reaction forces and force couple in a quasi-static case (unmodified gear).

time-varying line of action force, there is a time-varying displacement of the centre of this gear wheel in the same direction. This displacement is coupled to the rotation of the other gear wheel which affects the transmission error. This effect is not seen in a purely torsional model, cf. Ref. [17].

In the next case, dynamic effects are taken into account by applying a rotational speed that corresponds to a mesh frequency of 200 Hz. In Fig. 5, the curves corresponding to the curves in Fig. 2 are viewed. In the first plot, the shape of the curves look almost the same. However the dashed curve ($\mu = 0$) is somewhat lagging behind. It is interesting to note that the curve for d_y^2 still reminds one of the corresponding curve in Fig. 2.

In Fig. 6 the peak-to-peak value of the dynamic transmission error (T_{EPP}) is plotted as a function of the mesh frequency where it is also seen that for high mesh frequencies the dynamic transmission error is less than the static transmission error (cf. Fig. 2). It can be concluded that in this case, the presence of friction always increases T_{EPP}.

In order to reduce the effect from mesh stiffness variations, different kinds of profile modifications are used, see e.g. Ref. [1]. In Fig. 7, material is removed from parts of the flank that are loaded when two pairs of teeth are in contact. The modification is measured along the normal direction of the unmodified gear flank. In this model, profile modifications are included in the initial gaps g_j.

In the last case, a profile modification will be studied which is linear in the roll angle, see Eq. (A.1) in the appendix. The maximum modification depth, which is the same for pinion and gear, will be at the tip of the gear tooth. The modification starts at the highest point of single tooth contact (*HPSTC*). The roll angle at *HPSTC* is 29.61° for the pinion and 27.64° for the gear. The modification used here is of the same type as used in Ref. [7]. The interaction between the mesh

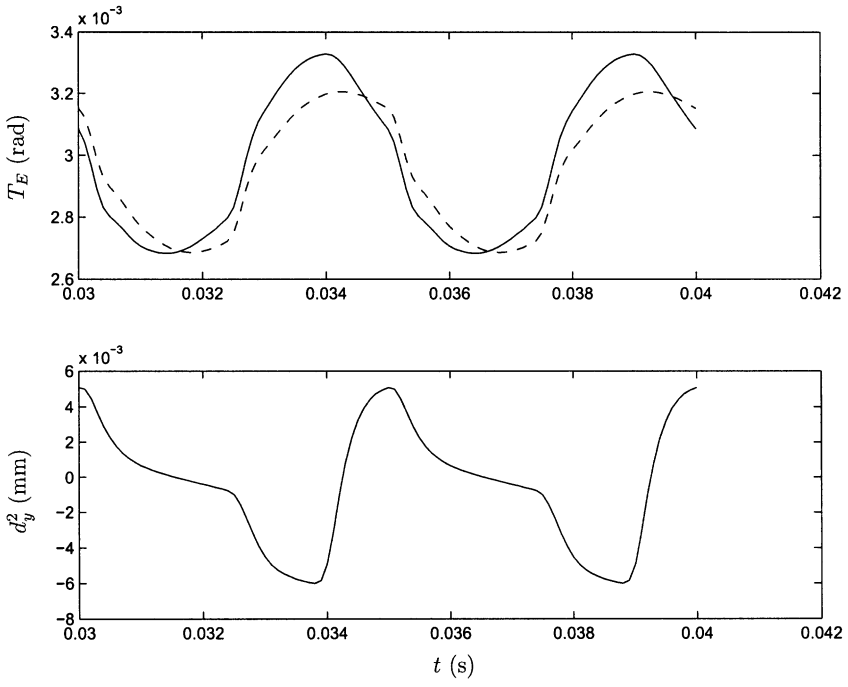

Fig. 5. Dynamic transmission error and shaft deflection d_y^2 of the left shaft (two mesh cycles). Solid line: $\mu = 0.1$ and dashed line: $\mu = 0$.

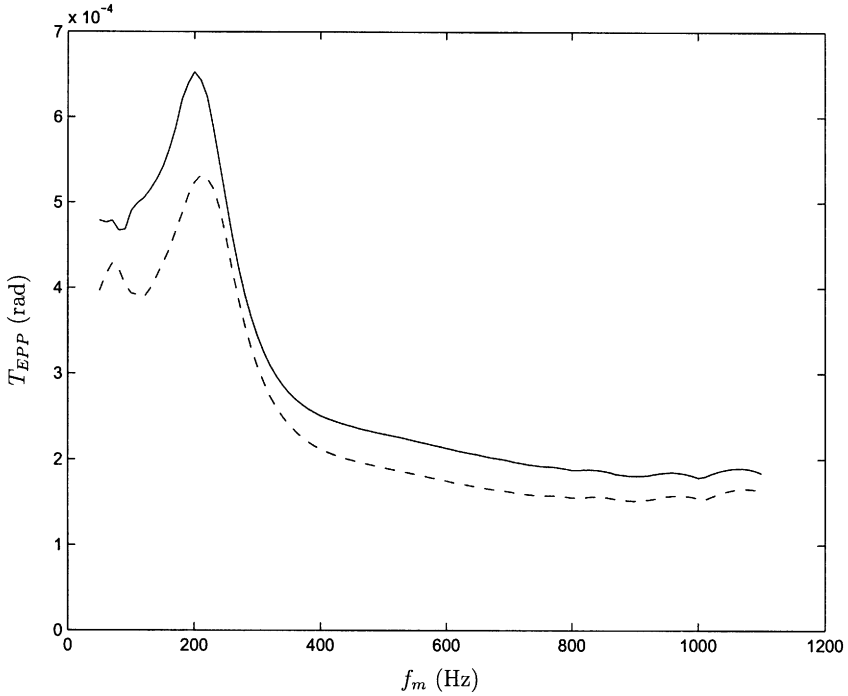

Fig. 6. Peak-to-peak dynamic transmission error versus mesh frequency. Solid line: $\mu = 0.1$ and dashed line: $\mu = 0$.

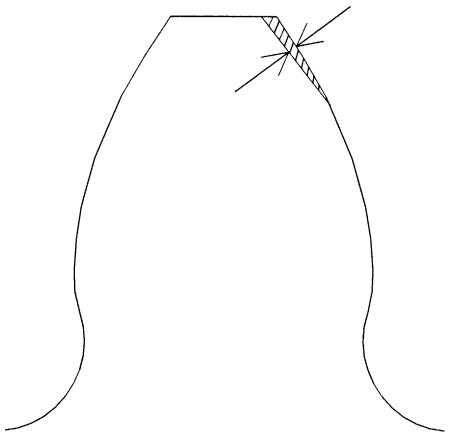

Fig. 7. Profile modification.

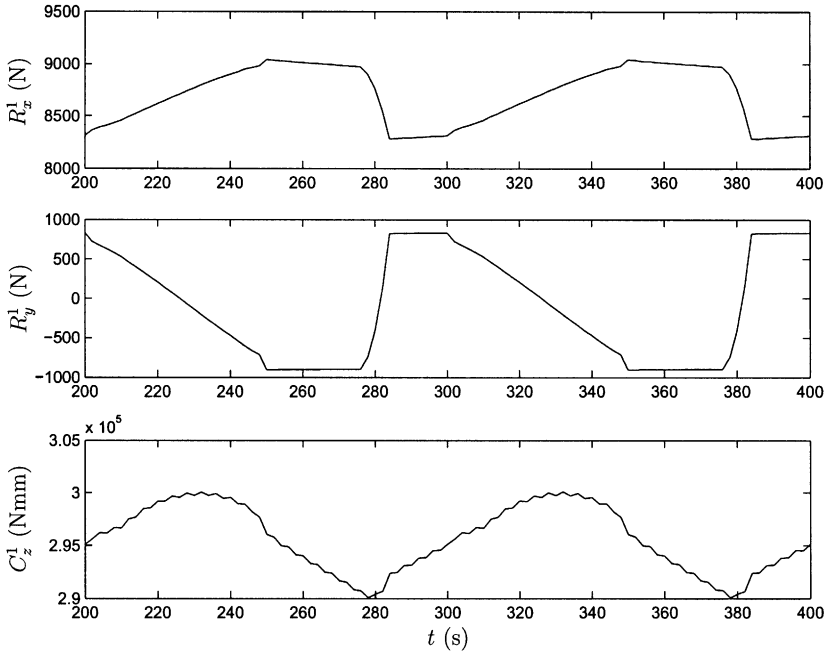

Fig. 8. Reaction forces and force couple in a quasi-static case for a modified gear with a maximum modification depth of 31 μm.

forces is viewed in Fig. 8. The curve of the total friction force, i.e., R_y^1, has almost the same appearance as the one achieved in Ref. [7] when Coulomb friction was used.

In Fig. 9, T_{EPP} is calculated for different profile modifications. In this figure it can be seen that the optimal value for the modification depends on whether friction is included or

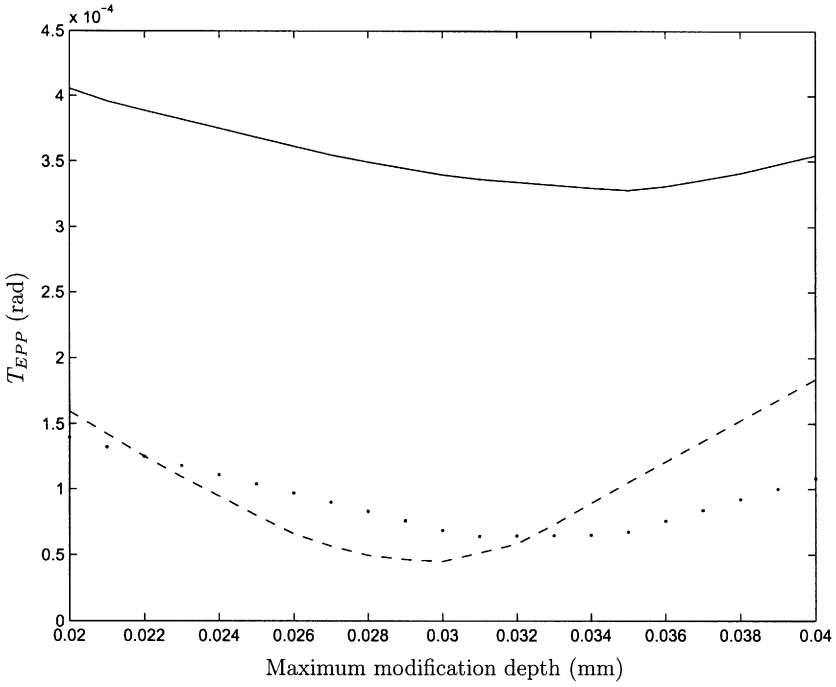

Fig. 9. T_{EPP} versus maximum modification depth. Solid line: mesh frequency 200 Hz with $\mu = 0.1$, dashed line: mesh frequency 200 Hz with $\mu = 0$ and dotted line: mesh frequency 0.01 Hz with $\mu = 0$ (static).

not. However, the differences are relatively small. Therefore, in gear design, it is reasonable to neglect friction and calculate static T_{EPP} in order to optimize the profile modification. By comparing Figs. 6 and 10 it can be seen that the improvement achieved by the profile modification is less significant when friction is included.

6. Conclusions and discussion

In this work a flexible multi-body model is developed where the main idea is to represent the contact interface in a gear mesh accurately enough to account for profile modifications and manufacturing errors, which are both in the order of 5–50 μm. The dynamic response of such a model is the main result, where the flank geometries, the mesh stiffness variations as well as friction are the sources of force excitation. The effect of friction is emphasised and it is concluded that it has an effect even on the motion in the rotational direction. The dynamic transmission error was calculated for a large number of mesh frequencies. It is noticeable that the dynamic transmission error is less than the static one at high mesh frequencies that are far from natural frequencies. By studying different amounts of profile modification it is concluded that optimal values for the profile modification are not the same depending on whether frictional effects are included or not. It is also concluded that the possibility to decrease the dynamic transmission error by applying profile modifications is reduced in the case of friction.

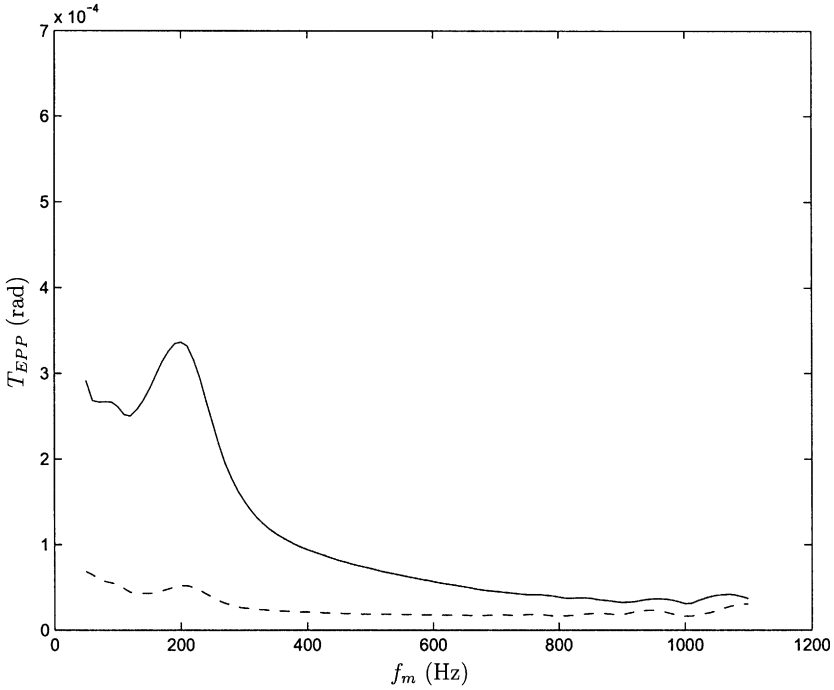

Fig. 10. Peak-to-peak dynamic transmission error versus mesh frequency for a gear with a maximum modification depth of 31 μm. Solid line: $\mu = 0.1$ and dashed line: $\mu = 0$.

The model data used in the numerical analyses have somewhat exaggerated values. The friction coefficient is somewhat too large and the lowest natural frequency is too low. The particular choice of these parameters is such that the properties of the system should appear better. However, in the model itself any value of the above are of course applicable. In order to verify the model the Load Distribution Program (LDP) [26] is used and good agreement was achieved for a quasi-static case with no friction. In a quasi-static case with friction, the total friction force for a modified gear is viewed in Fig. 8. This curve is compared with the one calculated in Ref. [7], where the total friction force was predicted for a gear with a similar type of modification, assuming Coulomb friction. Of course, a direct comparison is not possible but the appearances of the curves have a remarkable resemblance. In the dynamic cases studied in this work, it can be concluded that friction always tends to increase the peak-to-peak transmission error. This conclusion can also be drawn by studying the results presented in Ref. [8].

In this work only spur gears are treated in order to demonstrate the method and to predict some qualitative results. The method is however not restricted to the two-dimensional case. In general, helical gears are used exclusively in gearboxes today and to study gears with a helix angle is therefore a topic for further work.

Acknowledgements

This work was supported by CENIIT and Scania CV AB.

Appendix A. Interpolation—remeshing

When $\dot{\mathbf{u}}^i$ is approximated in Eq. (15) a difficulty arises due to the remeshing performed at every new time t_{n+1}. For a displacement $\mathbf{u}^i(\mathbf{Q}(t_{n+1})\mathbf{X}_j^i, t_{n+1})$ at a node defined by the position vector $\mathbf{X}_j^i$ the corresponding nodal displacement $\mathbf{u}^i(\mathbf{Q}(t_n)\mathbf{X}_j^i, t_n)$ do not necessarily exist due to a different mesh at time t_n compared to the mesh used at time t_{n+1}. This difficulty is treated by the approach outlined in this appendix. Notations used are defined by Fig. 11.

For a given gear flank, a material point is uniquely defined by the roll angle. The roll angle is given by

$$\vartheta_j^i = \frac{\sqrt{(r_j^i)^2 - (r_b)^2}}{r_b}, \tag{A.1}$$

where r_j^i is the radius of the material point identified by the position vector $\mathbf{X}_j^i$. The roll angle is the sum of the involute polar angle ψ and the pressure angle ξ. Thus, for each time t_n there exists a set $\mathcal{N}_n^i = \{\vartheta_1^i, \ldots, \vartheta_\xi^i\}$ defining the nodes of the contact surface. For a nodal displacement $\mathbf{u}^i(\vartheta_j^i, t_{n+1}) = \mathbf{u}_c^i(\mathbf{Q}(t_{n+1})\mathbf{X}_j^i, t_{n+1})$ the corresponding ϑ_j^i is checked against $\mathcal{N}_n^i$ in order to find $\vartheta_l^i < \vartheta_j^i < \vartheta_{l+1}^i$. Then, $\mathbf{u}_c^i(\vartheta_j^i, t_n)$ is approximated according to

$$\mathbf{u}^i(\vartheta_j^i, t_n) \simeq (1-\eta)\mathbf{u}^i(\vartheta_l^i, t_n) + \eta\mathbf{u}^i(\vartheta_{l+1}^i, t_n), \tag{A.2}$$

where

$$\eta = \frac{\vartheta_j^i - \vartheta_l^i}{\vartheta_{l+1}^i - \vartheta_l^i}. \tag{A.3}$$

If $\vartheta_l^i = \vartheta_j^i$, then, of course, $\mathbf{u}^i(\vartheta_j^i, t_n) = \mathbf{u}^i(\vartheta_l^i, t_n)$. If $\vartheta_j^i \notin [\vartheta_1^i, \vartheta_\xi^i]$, then the following approximation is adopted:

$$\mathbf{u}^i(\vartheta_j^i, t_n) \simeq \begin{bmatrix} 0 & -\varphi^i & 0 \\ \varphi^i & 0 & 0 \\ 0 & 0 & 0 \end{bmatrix} \mathbf{Q}(\omega t_n)\mathbf{X}_j^i + \begin{Bmatrix} d_x^i \\ d_y^i \\ 0 \end{Bmatrix}. \tag{A.4}$$

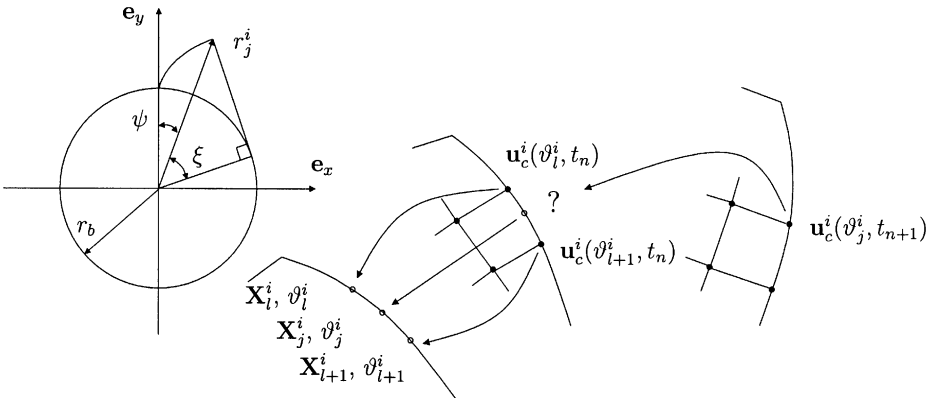

Fig. 11. The interpolation using the geometry of the involute gear.

This latter approximation might be arguable. A nicer approach would be to treat all nodes on the gear flanks as contact nodes. However, such an approach would be more time consuming and achieving a node-to-node condition would then be somewhat cumbersome.

Appendix B. Newton algorithm

Let

$$\mathbf{H}(\mathbf{y}) = \mathbf{0}$$

express the non-smooth equations (24), (25) and (C.1). This system of equations is solved using the following algorithm:

Algorithm. Let $\beta = 0.9$, $\gamma = 0.1$ and ε small. Repeat the following steps for each time t_{n+1}:

1. Let $\mathbf{y}^0$ be the solution from the previous time t_n and set $q = 0$.
2. Find a search direction $\mathbf{z}$ such that

$$\mathbf{H}(\mathbf{y}^q) + \mathbf{H}'(\mathbf{y}^q; \mathbf{z}) = \mathbf{0},$$

   where $\mathbf{H}'(\mathbf{y}^q; \mathbf{z})$ is the directional derivative. Explicit expression for this directional derivative can be found in e.g. Ref. [15].
3. Let $\alpha^q = \beta^{m_q}$, where m_q is the smallest integer $0 \leqslant m \leqslant 22$ for which the following decrease criterion holds:

$$\Phi(\mathbf{y}^q + \beta^m \mathbf{z}) \leqslant (1 - 2\gamma\beta^m)\Phi(\mathbf{y}^q), \quad \Phi(\mathbf{y}) = \tfrac{1}{2}\mathbf{H}^{\mathrm{T}}(\mathbf{y})\mathbf{H}(\mathbf{y}).$$

4. Set $\mathbf{y}^{q+1} = \mathbf{y}^q + \alpha^q \mathbf{z}$.
5. If $\Phi(\mathbf{y}^{q+1}) \leqslant \varepsilon$, then terminate with $\mathbf{y}^{q+1}$ as an approximate zero of $\mathbf{H}(\mathbf{y})$. Otherwise, replace q by $q + 1$ and return to step 1.

Appendix C. Reducing to $\bar{\mathbf{u}}_c$

By performing a static condensation, Eq. (22) can formally be written as

$$\begin{bmatrix} \mathbf{K}_c^1 & \mathbf{0} \\ \mathbf{0} & \mathbf{K}_c^2 \end{bmatrix} \begin{Bmatrix} \mathbf{u}_c^1 \\ \mathbf{u}_c^2 \end{Bmatrix} + \begin{Bmatrix} \mathbf{F}_c^1 \\ \mathbf{F}_c^2 \end{Bmatrix} + \begin{Bmatrix} \mathbf{F}_e^1 \\ \mathbf{F}_e^2 \end{Bmatrix} = \begin{Bmatrix} \mathbf{0} \\ \mathbf{0} \end{Bmatrix},$$

where $\mathbf{K}_c^i$ represents resulting stiffness matrices and $\mathbf{F}_e^i$ presents the external forces. By using the definition of $\bar{\mathbf{u}}_c$ and $\mathbf{F}_c^1 = -\mathbf{F}_c^2$, this may be written as

$$\begin{bmatrix} \mathbf{K}_c^1 & \mathbf{K}_c^1 \\ \mathbf{0} & \mathbf{K}_c^2 \end{bmatrix} \begin{Bmatrix} \bar{\mathbf{u}}_c \\ \mathbf{u}_c^2 \end{Bmatrix} + \begin{Bmatrix} \mathbf{F}_c^1 \\ -\mathbf{F}_c^1 \end{Bmatrix} + \begin{Bmatrix} \mathbf{F}_e^1 \\ \mathbf{F}_e^2 \end{Bmatrix} = \begin{Bmatrix} \mathbf{0} \\ \mathbf{0} \end{Bmatrix}.$$

Now, by adding the first row to the second row, one obtains

$$\begin{bmatrix} \mathbf{K}_c^1 & \mathbf{K}_c^1 \\ \mathbf{K}_c^1 & \mathbf{K}_c^1 + \mathbf{K}_c^2 \end{bmatrix} \begin{Bmatrix} \bar{\mathbf{u}}_c \\ \mathbf{u}_c^2 \end{Bmatrix} + \begin{Bmatrix} \mathbf{F}_c^1 \\ \mathbf{0} \end{Bmatrix} + \begin{Bmatrix} \mathbf{F}_e^1 \\ \mathbf{F}_e^1 + \mathbf{F}_e^2 \end{Bmatrix} = \begin{Bmatrix} \mathbf{0} \\ \mathbf{0} \end{Bmatrix}.$$

Finally, by reducing $\mathbf{u}_c^2$, one arrives at

$$[\mathbf{K}_c^1 - \mathbf{K}_c^1[\mathbf{K}_c^1 + \mathbf{K}_c^2]^{-1}\mathbf{K}_c^1]\bar{\mathbf{u}}_c + \mathbf{F}_c^1 + \mathbf{F}_e^1 - \mathbf{K}_c^1[\mathbf{K}_c^1 + \mathbf{K}_c^2]^{-1}\{\mathbf{F}_e^1 + \mathbf{F}_e^2\} = \mathbf{0}. \tag{C.1}$$

In the numerical implementation Eqs. (24), (25) and (C.1) define the augmented Lagrangian system which is solved using the algorithm presented in Appendix B.

Appendix D. Nomenclature

C	force couple
$\mathbf{C}$	transformation matrix
E	Young's modulus
$\mathbf{F}$	column vector of forces and moments
J	mass moment of inertia
$\mathbf{K}$	stiffness matrix
$\mathbf{P}$	column vector of nodal contact forces
$\mathbf{Q}$	rotation matrix
R	reaction force
T_E	transmission error
$\mathbf{X}$	position vector in reference configuration
Z	number of teeth
$\mathbf{c}$	position vector of gear centre
d	displacement of gear centre
$\mathbf{e}$	base vector
f_m	mesh frequency
g	initial gap
k_b	translational stiffness
k_s	torsional stiffness
m	mass
p	nodal contact force
t	time
u	nodal displacement
$\mathbf{u}$	nodal displacement vector
$\mathbf{v}^{rigid}$	column vector of rigid relative nodal velocities
$\dot{w}$	relative nodal velocity
$\mathbf{x}$	position vector in current configuration
α	stiffness proportional damping coefficient
β	mass proportional damping coefficient
θ	prescribed rotation
μ	coefficient of friction

v	Poisson's ratio
φ	infinitesimal rotation
ω	angular velocity

Subscripts

c	finite element degrees of freedom of potential contact surface
d	finite element degrees of freedom
j	node pair reference number
n	normal direction
q	degrees of freedom of shaft system
t	tangential direction
x, y, z	global co-ordinate directions

Superscripts

i	reference to pinion ($i = 1$) and gear ($i = 2$)
T	matrix transpose

References

[1] D.P. Townsend, *Dudley's Gear Handbook*, 2nd Edition, McGraw-Hill, New York, 1992.
[2] N. Özgüven, D.R. Houser, Mathematical models used in gear dynamics—a review, *Journal of Sound and Vibration* 121 (1988) 383–411.
[3] R.G. Parker, S.M. Vijayakar, T. Imajo, Non-linear dynamic response of a spur gear pair: modelling and experimental comparisons, *Journal of Sound and Vibration* 237 (2000) 435–455.
[4] A. Bajer, L. Demkowicz, Dynamic contact/impact problems, energy conservation and planetary gear trains, *Computer Methods in Applied Mechanics and Engineering* 191 (2002) 4159–4191.
[5] P. Velex, M. Maatar, A mathematical model for analysing the influence of shape deviations and mounting errors on gear dynamic behavior, *Journal of Sound and Vibration* 191 (1996) 629–660.
[6] D. Hochmann, D.R. Houser, Friction force as a dynamic excitation source in involute spur and helical gearing, *Proceedings of the Eighth International Power Transmission and Gearing Conference*, vol. DETC2000/PTG:14429, Baltimore, MD, 2000.
[7] M. Vaishya, D.R. Houser, Modeling and analysis of sliding friction in gear dynamics, *Proceedings of the Eighth International Power Transmission and Gearing Conference*, DETC2000/PTG:14431, Baltimore, MD, 2000.
[8] P. Velex, V. Cahouet, Experimental and numerical investigations on the influence of tooth friction in spur and helical gear dynamics, *Journal of Mechanical Design* 122 (2000) 515–522.
[9] M. Vaishya, R. Singh, Analysis of periodically varying gear mesh systems with Coulomb friction using Floquet theory, *Journal of Sound and Vibration* 243 (3) (2001) 525–545.
[10] P. Velex, P. Sainsot, An analytical study of tooth friction excitations in errorless spur and helical gears, *Mechanism and Machine Theory* 37 (2002) 641–658.
[11] T.A. Laursen, V. Chawla, Design of energy conserving algorithms for frictionless contact problems, *International Journal for Numerical Methods in Engineering* 40 (1997) 863–866.
[12] P. Alart, A. Curnier, A mixed formulation for frictional contact problems prone to Newton like solution methods, *Computer Methods in Applied Mechanics and Engineering* 92 (1991) 353–375.
[13] A. Klarbring, Mathematical programming and augmented Lagrangian methods for frictional contact problems, in: A. Curnier (Ed.), *Proceedings of Contact Mechanics International Symposium*, 1992, pp. 409–422.
[14] N. Strömberg, An augmented Lagrangian method for fretting problems, *European Journal of Mechanics, A/Solids* 16 (1997) 573–593.

[15] P.W. Christensen, A. Klarbring, J.S. Pang, N. Strömberg, Formulation and comparison of algorithms for frictional contact problems, *International Journal for Numerical Methods in Engineering* 42 (1998) 145–173.
[16] O. Lundvall, A. Klarbring, Simulation of wear by use of a non-smooth Newton method—a spur gear application, *Mechanics of Structures and Machines* 29 (2001) 223–238.
[17] O. Lundvall, A. Klarbring, Prediction of transmission error in spur gears as a consequence of wear using FEM, *Mechanics of Structures and Machines* 29 (2001) 431–449.
[18] A.A. Shabana, *Dynamics of Multibody Systems*, Cambridge University Press, Cambridge, 1998.
[19] T.A. Laursen, *Computational Contact and Impact Mechanics, Fundamentals of Modeling Interfacial Phenomena in Nonlinear Finite Element Analysis*, Springer, Berlin, 2002.
[20] P. Wriggers, *Computational Contact Mechanics*, Wiley, New York, 2002.
[21] P. Ireman, A. Klarbring, N. Strömberg, Finite element algorithms for thermoelastic wear problems, *European Journal of Mechanics, A/Solids* 21 (2002) 423–440.
[22] N. Strömberg, A Newton method for three-dimensional fretting problems, *International Journal of Solids and Structures* 36 (1999) 2075–2090.
[23] L. Johansson, A. Klarbring, Study of frictional impact using a nonsmooth equation solver, *Journal of Applied Mechanics* 67 (2000) 267–273.
[24] P.W. Christensen, A semi-smooth Newton method for elasto-plastic contact problems, *International Journal of Solids and Structures* 39 (2002) 2323–2341.
[25] N. Strömberg, A method for structural dynamic contact problems with friction and wear, *International Journal of Numerical Methods in Engineering* 58 (2003) 2371–2385.
[26] GearLab, Ohio State University, *Load Distribution Program*, Version 10.8.